JOURNAL OF COMPUTATIONAL PHYSICS 88, 305–336 (1990)

Solutions of Reynolds-Averaged Navier–Stokes Equations for Three-Dimensional Incompressible Flows

H. C. CHEN, V. C. PATEL, AND S. JU

Iowa Institute of Hydraulic Research,
The University of Iowa,

Iowa City, Iowa 52242–1585

Received August 15, 1988; revised April 28, 1989

A general numerical method for the solution of complete Reynolds-averaged Navier–Stokes equations for three-dimensional flows is described. The method uses nonorthogonal body-fitted coordinates, generated either analytically or numerically, while retaining the velocity components in a triply-orthogonal curvilinear coordinate system. The convective transport equations for mean velocities and turbulence parameters (k, ε) are solved by the finite-analytic method in the transformed domain. The pressure field is updated using a modified version of the SIMPLER algorithm to satisfy the equation of continuity. The capability of the method and its overall performance are demonstrated by calculations of the flow over a typical ship hull.

INTRODUCTION

Numerical solutions of the complete Navier–Stokes equations for laminar flow and the corresponding Reynolds-averaged equations for turbulent flow have received a great deal of attention in recent years since, in principle, they describe flows with any level of complexity, the only uncertainty being that introduced by the turbulence model employed to effect closure of the Reynolds equations. Indeed, solutions using a variety of numerical schemes are becoming quite common for flows involving two-dimensional and axisymmetric geometries or some other simplifying features. As available computing power increases, many problems of practical interest, which invariably involve complex three-dimensional geometries, are becoming tractable through solutions of the complete equations. The rapid progress being made in numerical generation of computational grids for arbitrary bodies greatly facilitate such applications.

Computational fluid dynamics (CFD) is beginning to play a major role in analysis and design for applications in aerodynamics, turbomachinery, ship hydrodynamics, and many other branches of fluid mechanics. A number of review articles presented at the AIAA 8th CFD conference [1] provide an overview of CFD applications in aircraft and automobile industries. Applications in turbomachinery were also reviewed in the above references as well as in McNally and

0021-9991/90 $3.00

Sockol [2], while recent advances in some applications in ship hydrodynamics have been summarized by Patel [3]. The numerical methods used in these applications are appropriate for equations ranging from the Euler equations for inviscid flows to the complete Reynolds-averaged Navier–Stokes equations for turbulent compressible flows. An assessment of these and other related finite-difference methods has been made in Refs. [4–6].

It is of interest to note here that considerable confusion abounds in the terminology used in the literature, particularly with regard to the term "Navier–Stokes." In addition to the complete Reynolds-averaged equations for turbulent flow, it is often associated, rather loosely and incorrectly, with equations in which further approximations are made. In the numerical solutions for general three-dimensional viscous flows, we can distinguish at least three levels of approximations between the classical boundary-layer equations and the complete Navier–Stokes equations. A set of second-order boundary-layer equations can be deduced by formally retaining the second-order terms in the familiar order-of-magnitude analysis (Nash and Patel [7]). A greater degree of generality is embodied in the somewhat inappropriately named "thin-layer" or "thin-layer Navier–Stokes" equations, in which all viscous and turbulent transport terms other than those in the direction normal to the surface are neglected. The next level of generality, beyond which lies the complete equations, is achieved by the so-called partially-parabolic (or "parabolized Navier–Stokes," or "semi-elliptic Navier–Stokes") equations, in which only the longitudinal transport due to viscosity and turbulence is neglected. Here, we are concerned with solution of the complete equations without approximations of the above kind.

Despite the great strides made in CFD, numerical solutions of the complete Reynolds-averaged equations for general three-dimensional flows are still quite limited. Methods which appear to have this capability are those of Refs. [8–14] for compressible flows, and Refs. [14–16] for incompressible flows. Here, we focus our attention only on methods which deal with incompressible flows.

The assumption of incompressibility is appropriate for applications in hydrodynamics, meteorology, automobile aerodynamics, building aerodynamics, and other flows at low Mach numbers. As the speed of sound approaches infinity and the pressure in the equation of state is only weakly coupled with the continuity and momentum equations in the incompressible limit, the implementation of compressible-flow Navier–Stokes codes for simulating incompressible flows becomes inefficient and inaccurate. Consequently, methods capable of handling the direct coupling between velocity and pressure must be sought to ensure a divergence-free velocity field. Two different approaches, namely the pressure-correction and the artificial-compressibility methods, have been used to handle this coupling for general three-dimensional flows. In the pressure-correction methods, such as those proposed by Patankar and Spalding [17], Patankar [18], and Issa [19], the equation of continuity is enforced at every time step through the solution of a Poisson equation for pressure-correction or pressure itself. The artificial compressibility methods, proposed initially by Chorin [20], on the other hand, add a pseudo-

compressibility term in the equation of continuity and retain the numerical methodology used for compressible flows. The introduction of this nonphysical pseudocompressibility, however, precludes the use of these methods for the simulation of unsteady incompressible flows. A time-accurate algorithm based on artificial compressibility has been proposed recently by Merkle and Athavale [21], but current applications are limited to the two-dimensional Euler equations.

For three-dimensional flows involving complex geometries, it is desirable to employ body-fitted coordinate systems so that the flow in the wall layer can be accurately resolved with a reasonable number of grid points. Once such a coordinate system is selected for a given geometry, there remains the task of formulating the equations of motion in that system. Two different approaches can be adopted for this purpose. One of these uses that may be termed "partial transformations," in which only the independent coordinate variables are transformed, leaves the dependent variables (i.e., velocity components) in a preselected orthogonal coordinate system. This approach, which has been used by Chen and Patel [22–24], Rhie [14], and Han [16], among others, has the advantages that the resulting equations have a strong conservation form and facilitate the use of pressure-velocity coupling algorithms based on conservation of mass. Also, the equations are relatively simple, and the results can be readily interpreted. Since the velocity vectors, in general, do not align with the coordinate directions, this approach may lead to increased numerical diffusion when the angles between the velocity components and coordinate surfaces become large. The alternative is to transform the equations completely, including the independent as well as the dependent variables. This approach has been used by, among others, Richmond *et al.* [25], Stern *et al.* [26], Demirdzic *et al.* [27], and Ogawa and Ishiguro [28]. The use of contravariant velocity components in such a complete transformation allows a much more accurate resolution of the flow near a solid surface. However, the fully-transformed equations involve many more geometric coefficients and their higher-order derivatives. This not only leads to increased computer storage requirements but also can adversely affect the flow solution if the coefficients are not smooth and accurate. In many practical applications, it is not necessary to use the complete transformations if the basic coordinate systems are chosen carefully so as to avoid large skew angles between velocity components and the faces of the computational cell.

This paper is concerned with the development of a numerical method for the solution of Reynolds-averaged Navier–Stokes equations based on a partial transformation of the governing equations. For complete generality, the equations are written in the triply-orthogonal curvilinear coordinate system and transformed into a general nonorthogonal system. Closure of the Reynolds equations is effected by the two-equation $k-\varepsilon$ turbulence model. The transport equations of momentum and the two turbulence parameters are discretized using the finite-analytic scheme of Chen and Chen [29–31]. Pressure-velocity coupling is established via the continuity equation by a modified version of the SIMPLER algorithm of Patankar [18]. To demonstrate the capabilities of the method, calculations are

presented for the flow over a ship model. This requires resolution of the thin boundary layer over the middle part of the hull, its rapid thickening over the stern, and the evolution of the wake from such a complex turbulent shear flow.

Equations and Coordinates

(a) *Physical Plane*

We consider the equations of motion, in general triply-orthogonal curvilinear coordinates (x^1, x^2, x^3, t) for unsteady, three-dimensional, incompressible flow. The exact Reynolds-averaged equations of continuity and momentum [7, 25], in dimensionless form, are

$$\frac{1}{h_1 h_2 h_3}\left\{\frac{\partial}{\partial x^1}[h_2 h_3 V(1)]+\frac{\partial}{\partial x^2}[h_1 h_3 V(2)]+\frac{\partial}{\partial x^3}[h_1 h_2 V(3)]\right\}=0 \tag{1}$$

$$\begin{aligned}\frac{\partial V(i)}{\partial t}+\sum_{m=1}^{3}\Bigg\{&\frac{V(m)}{h_m}\frac{\partial V(i)}{\partial x^m}+[K_{im}V(i)-K_{mi}V(m)]\,V(m)+\frac{1}{h_m}\frac{\partial\overline{v(i)\,v(m)}}{\partial x^m}\\&+(2K_{im}+K_{jm}+K_{km}-K_{mm})\,\overline{v(i)\,v(m)}-K_{mi}\,\overline{v(m)\,v(m)}\Bigg\}+\frac{1}{h_i}\frac{\partial p}{\partial x^i}\\&-\frac{1}{\mathrm{Re}}\left\{\nabla^2 V(i)+\sum_{m=1}^{3}\left[\frac{2K_{im}}{h_i}\frac{\partial V(m)}{\partial x^i}-\frac{2K_{mi}}{h_m}\frac{\partial V(m)}{\partial x^m}+\alpha_{im}V(m)\right]\right\}=0,\end{aligned} \tag{2}$$

where

$$\begin{aligned}\nabla^2&=\frac{1}{h_1 h_2 h_3}\sum_{m=1}^{3}\frac{\partial}{\partial x^m}\left(\frac{h_1 h_2 h_3}{h_m^2}\frac{\partial}{\partial x^m}\right)\\&=\sum_{m=1}^{3}\left[\frac{1}{h_m^2}\frac{\partial^2}{\partial x^m\,\partial x^m}+(K_{1m}+K_{2m}+K_{3m}-2K_{mm})\frac{1}{h_m}\frac{\partial}{\partial x^m}\right]\end{aligned} \tag{3a}$$

and

$$K_{ij}=\frac{1}{h_i h_j}\frac{\partial h_i}{\partial x^j},\qquad i,j=1,2,3 \tag{3b}$$

are the curvature parameters and h_i are the coordinate metrics. α_{ij} are functions only of the curvature parameters and their derivatives,

$$\begin{aligned}\alpha_{ii}&=-(K_{ij}^2+K_{ji}^2+K_{ik}^2+K_{ki}^2)\\\alpha_{ij}&=\frac{1}{h_i}\frac{\partial K_{ij}}{\partial x^i}-\frac{1}{h_j}\frac{\partial K_{ji}}{\partial x^j}-K_{kj}(K_{ki}+K_{ji})+K_{ki}K_{ij}\\\alpha_{ik}&=\frac{1}{h_i}\frac{\partial K_{ik}}{\partial x^i}-\frac{1}{h_k}\frac{\partial K_{ki}}{\partial x^k}-K_{jk}(K_{ki}+K_{ji})+K_{ji}K_{ik},\end{aligned} \tag{4}$$

where i, j, k are in cyclic order, x^i are the dimensionless coordinates normalized by a characteristic length L, and t is the time normalized by L/U_0. $V(i) = (U, V, W)$ are the components of mean velocity normalized by the characteristic velocity U_0, p is the pressure normalized by ρU_0^2, $\mathrm{Re} = U_0 L/\nu$ is the Reynolds number defined in terms of U_0, L, and molecular kinematic viscosity ν. The barred quantities $\overline{v(i)\, v(m)}$, etc., are the turbulent Reynolds stresses, normalized by U_0^2.

The two-equation $k-\varepsilon$ turbulence model is used to model the Reynolds stresses. Each stress is related to the corresponding mean rate of strain by an isotropic eddy viscosity ν_t as

$$-\overline{v(m)\, v(n)} = 2\nu_t e(mn) - \tfrac{2}{3}\delta_{mn} k, \tag{5}$$

where $e(mn)$ are the physical components of the mean rate-of-strain tensor defined by

$$e(mn) = \frac{1}{2}\left\{\frac{1}{h_m}\frac{\partial V(n)}{\partial x^m} + \frac{1}{h_n}\frac{\partial V(m)}{\partial x^n} + \delta_{mn}\sum_{l=1}^{3}\left(K_{ml} + K_{nl}\right) V(l) - K_{mn} V(m) - K_{nm} V(n)\right\} \tag{6}$$

and δ_{mn} is the Kronecker delta. The eddy viscosity is related to the dimensionless turbulent kinetic energy k, and its rate of dissipation ε, by

$$\nu_t = C_\mu \frac{k^2}{\varepsilon}, \tag{7}$$

where C_μ is a constant, and k and ε are governed by the transport equations

$$\frac{\partial k}{\partial t} + \sum_{m=1}^{3}\left\{\frac{V(m)}{h_m}\frac{\partial k}{\partial x^m} - \frac{1}{h_m}\frac{\partial}{\partial x^m}\left(\frac{1}{R_k h_m}\frac{\partial k}{\partial x^m}\right)\right\} - G + \varepsilon = 0 \tag{8}$$

$$\frac{\partial \varepsilon}{\partial t} + \sum_{m=1}^{3}\left\{\frac{V(m)}{h_m}\frac{\partial \varepsilon}{\partial x^m} - \frac{1}{h_m}\frac{\partial}{\partial x^m}\left(\frac{1}{R_\varepsilon h_m}\frac{\partial \varepsilon}{\partial x^m}\right)\right\} - C_{\varepsilon 1}\frac{\varepsilon}{k} G + C_{\varepsilon 2}\frac{\varepsilon^2}{k} = 0. \tag{9}$$

G is the turbulence generation term defined by

$$G = 2\nu_t \sum_{m=1}^{3}\sum_{n=1}^{3} e(mn)\, e(mn). \tag{10}$$

The effective "Reynolds number," R_ϕ, for each of the five transport quantities ϕ is defined as

$$\frac{1}{R_\phi} = \frac{1}{\mathrm{Re}} + \frac{\nu_t}{\sigma_\phi}, \tag{11}$$

where $\phi = (U, V, W, k, \varepsilon)$ with $U = V(1)$, $V = V(2)$, and $W = V(3)$. The values of the constants in these equations are $C_\mu = 0.09$, $C_{\varepsilon 1} = 1.44$, $C_{\varepsilon 2} = 1.92$, $\sigma_U = \sigma_V = \sigma_W = \sigma_k = 1.0$, and $\sigma_\varepsilon = 1.3$.

Using Eqs. (5), (7), and (11), Eqs. (2), (8), and (9) can be written

$$\frac{\partial V(i)}{\partial t}+\sum_{m=1}^{3}\left\{\left[V(m)-\frac{1}{h_m}\frac{\partial v_t}{\partial x^m}\right]\frac{1}{h_m}\frac{\partial V(i)}{\partial x^m}-\frac{1}{h_m}\frac{\partial v_t}{\partial x^m}\left[\frac{1}{h_i}\frac{\partial V(m)}{\partial x^i}-K_{im}V(i)-K_{mi}V(m)\right]\right.$$
$$\left.-\frac{2}{h_i}\frac{\partial v_t}{\partial x^i}K_{im}V(m)+\left[K_{im}V(i)-K_{mi}V(m)\right]V(m)\right\}+\frac{1}{h_i}\frac{\partial}{\partial x^i}\left(p+\frac{2}{3}k\right)$$
$$-\frac{1}{R_\phi}\left\{\nabla^2 V(i)+\sum_{m=1}^{3}\left[\frac{2K_{im}}{h_i}\frac{\partial V(m)}{\partial x^i}-\frac{2K_{mi}}{h_m}\frac{\partial V(m)}{\partial x^m}+\alpha_{im}V(m)\right]\right\}=0 \tag{12}$$

$$\frac{\partial k}{\partial t}+\sum_{m=1}^{3}\left[V(m)-\frac{1}{\sigma_k h_m}\frac{\partial v_t}{\partial x^m}\right]\frac{1}{h_m}\frac{\partial k}{\partial x^m}-\frac{1}{R_k}\nabla^2 k-G+\varepsilon=0 \tag{13}$$

$$\frac{\partial \varepsilon}{\partial t}+\sum_{m=1}^{3}\left[V(m)-\frac{1}{\sigma_\varepsilon h_m}\frac{\partial v_t}{\partial x^m}\right]\frac{1}{h_m}\frac{\partial \varepsilon}{\partial x^m}-\frac{1}{R_\varepsilon}\nabla^2\varepsilon-C_{\varepsilon 1}\frac{\varepsilon}{k}G+C_{\varepsilon 2}\frac{\varepsilon^2}{k}=0. \tag{14}$$

It is convenient to rewrite these in the compact form,

$$\nabla^2\phi=R_\phi\left(\sum_{m=1}^{3}\frac{\alpha_\phi^m}{h_m}\frac{\partial\phi}{\partial x^m}+\frac{\partial\phi}{\partial t}\right)+s_\phi \tag{15}$$

with

$$\alpha_\phi^m=V(m)-\frac{1+\beta_\phi^m}{\sigma_\phi h_m}\frac{\partial v_t}{\partial x^m} \tag{16}$$

and

$$\beta_\phi^m=\begin{cases}1, & \text{for } \beta_U^1,\ \beta_V^2,\ \beta_W^3\\ 0, & \text{otherwise,}\end{cases} \tag{17}$$

where ϕ again represents any one of the convective transport quantities: $(U, V, W, k, \varepsilon)$. The source functions s_ϕ for $U=V(1)$, $V=V(2)$, $W=V(3)$, k, and ε are, respectively,

$$s_\phi=\frac{R_\phi}{h_i}\frac{\partial}{\partial x^i}\left(p+\frac{2}{3}k\right)+\sum_{m=1}^{3}\left\{\frac{R_\phi}{h_m}\frac{\partial v_t}{\partial x^m}\left[\frac{\beta_\phi^i-1}{h_i}\frac{\partial V(m)}{\partial x^i}+K_{im}V(i)+K_{mi}V(m)\right]\right.$$
$$-\frac{2R_\phi}{h_i}\frac{\partial v_t}{\partial x^i}K_{im}V(m)+R_\phi\left[K_{im}V(i)-K_{mi}V(m)\right]V(m)+\frac{2K_{mi}}{h_m}\frac{\partial V(m)}{\partial x^m}$$
$$\left.-\frac{2K_{im}}{h_i}\frac{\partial V(m)}{\partial x^i}-\alpha_{im}V(m)\right\}\qquad(\phi\equiv U, V, W) \tag{18a}$$

$$s_k=-R_k(G-\varepsilon) \tag{18b}$$

$$s_\varepsilon=-R_\varepsilon\frac{\varepsilon}{k}(C_{\varepsilon 1}G-C_{\varepsilon 2}\varepsilon). \tag{18c}$$

Equations (12) through (14) are five coupled, nonlinear, partial differential equations and, together with the continuity equation (1), are sufficient, in principle, to solve for the six unknowns p, U, V, W, k, and ε when proper initial and boundary conditions are specified.

(b) *Transformed Plane*

For the flow around three-dimensional bodies, orthogonal coordinates are not the most convenient or efficient for numerical solutions. It is, therefore, desirable to introduce analytic or numerical coordinate transformations which simplify the computational domain in the transformed plane and facilitate applications of the boundary conditions. Here, we adopt a body-fitted coordinate system since it offers the advantages of generality and flexibility and, most importantly, transforms the computational domain into a simple rectangular region with equal grid spacing.

The basic idea is to find a transformation such that the boundary surface of the physical domain in the orthogonal coordinate system (x^1, x^2, x^3, t) are transformed into boundaries of a simple rectangular domain in the computational space $(\xi^1, \xi^2, \xi^3, \tau) = (\xi, \eta, \zeta, \tau)$, as shown in Fig. 1. Once the body-fitted coordinate system is generated, either analytically or numerically, the corresponding transformation rules can be readily obtained from the specific transformations $t = \tau$, $x^i = x^i(\xi, \eta, \zeta, \tau)$. In particular, the usual vector operations for dependent variables can be expressed in terms of (ξ, η, ζ, τ) as

$$\nabla\phi = \frac{1}{h_i}\frac{\partial\phi}{\partial x^i} = \frac{1}{J}\sum_{l=1}^{3} b_i^l \frac{\partial\phi}{\partial\xi^l} \tag{19}$$

$$\nabla^2\phi = \sum_{m=1}^{3}\sum_{n=1}^{3} g^{mn}\frac{\partial^2\phi}{\partial\xi^m\partial\xi^n} + \sum_{m=1}^{3} f^m \frac{\partial\phi}{\partial\xi^m} \tag{20}$$

$$\frac{\partial\phi}{\partial t} = \frac{\partial\phi}{\partial\tau} - \frac{1}{J}\sum_{m=1}^{3}\sum_{n=1}^{3} b_n^m V_g(n)\frac{\partial\phi}{\partial\xi^m} \tag{21}$$

with $V_g(n) = h_n(\partial x^n/\partial\tau)$, where $V_g(n)$ are the grid velocities of the moving coordinate system, and the geometric coefficients b_i^j, g^{ij}, and f^i are defined by

$$b_i^l = \frac{J}{h_i}\frac{\partial\xi^l}{\partial x^i} = h_j h_k\left(\frac{\partial x^j}{\partial\xi^m}\frac{\partial x^k}{\partial\xi^n} - \frac{\partial x^k}{\partial\xi^m}\frac{\partial x^j}{\partial\xi^n}\right) \tag{22}$$

$$g^{li} = \sum_{p=1}^{3} b_p^l b_p^i = \frac{1}{J^2}(g_{mj}g_{nk} - g_{mk}g_{nj}) \tag{23}$$

$$f^l = \frac{1}{J}\sum_{p=1}^{3}\frac{\partial}{\partial\xi^p}(Jg^{lp}) \tag{24}$$

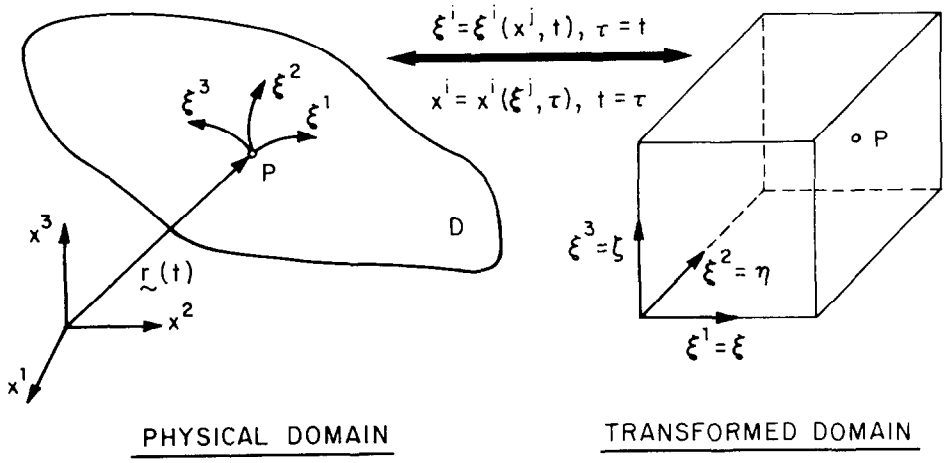

FIG. 1. Coordinate transformation between physical and numerical planes.

with both (i, j, k) and (l, m, n) in cyclic order. The metric tensor g^{ij} and Jacobian J are, respectively,

$$g_{ij} = \sum_{m=1}^{3} h_m^2 \frac{\partial x^m}{\partial \xi^i} \frac{\partial x^m}{\partial \xi^j} \tag{25a}$$

$$J^2 = \det(g_{ij}) = g_{11}g_{22}g_{33} + 2g_{12}g_{13}g_{23} - g_{11}(g_{23})^2 - g_{22}(g_{13})^2 - g_{33}(g_{12})^2. \tag{25b}$$

Using the above relations, Eq. (15) can be rearranged into a general convective transport equation of the form

$$\sum_{m=1}^{3} \left(g^{mm} \frac{\partial^2 \phi}{\partial \xi^m \partial \xi^m} - 2a_\phi^m \frac{\partial \phi}{\partial \xi^m} \right) = R_\phi \phi_\tau + S_\phi, \tag{26}$$

where

$$2a_\phi^m = \frac{R_\phi}{J} \sum_{n=1}^{3} b_n^m [\alpha_\phi^n - V_g(n)] - f^m \tag{27a}$$

$$\alpha_\phi^n = V(n) - \frac{1 + \beta_\phi^n}{J\sigma_\phi} \sum_{l=1}^{3} b_n^l \frac{\partial v_l}{\partial \xi^l} \tag{27b}$$

$$S_\phi = s_\phi - 2(g^{12}\phi_{\xi\eta} + g^{13}\phi_{\xi\zeta} + g^{23}\phi_{\eta\zeta}) \tag{27c}$$

and β_ϕ^n are as defined in Eq. (17). Hereafter, the subscripts (ξ, η, ζ, τ) on

ϕ ($= U, V, W, k, \varepsilon$) and v_t denote derivatives. The source functions s_ϕ can also be expressed in terms of $(\xi, \eta, \zeta, \tau) = (\xi^1, \xi^2, \xi^3, \tau)$ in the transformed plane as

$$s_\phi = \frac{1}{J}\sum_{m=1}^{3}\sum_{n=1}^{3}\left\{R_\phi b_m^n \frac{\partial v_t}{\partial \xi^n}\left[\frac{\beta_\phi^i - 1}{J}\sum_{l=1}^{3} b_i^l \frac{\partial V(m)}{\partial \xi^l} + K_{im}V(i) + K_{mi}V(m)\right]\right.$$
$$- 2R_\phi b_i^n \frac{\partial v_t}{\partial \xi^n} K_{im}V(m) + 2(K_{mi}b_m^n - K_{im}b_i^n)\frac{\partial V(m)}{\partial \xi^n}\Big\}$$
$$+ \sum_{m=1}^{3}\left\{\frac{R_\phi}{J} b_i^m \frac{\partial}{\partial \xi^m}\left(p + \frac{2}{3}k\right) + R_\phi[K_{im}V(i) - K_{mi}V(m)]\,V(m)\right.$$
$$\left. - \alpha_{im}V(m)\right\} \qquad (\phi \equiv U, V, W) \tag{28a}$$

$$s_k = -R_k(G - \varepsilon) \tag{28b}$$

$$s_\varepsilon = -R_\varepsilon \frac{\varepsilon}{k}(c_{\varepsilon 1}G - c_{\varepsilon 2}\varepsilon), \tag{28c}$$

where the turbulence generation G is given by Eq. (10) with

$$e(mn) = \frac{1}{2}\left\{\sum_{l=1}^{3}\left[\frac{1}{J}b_m^l \frac{\partial V(n)}{\partial \xi^l} + \frac{1}{J}b_n^l \frac{\partial V(m)}{\partial \xi^l} + \delta_{mn}(K_{ml} + K_{nl})\,V(l)\right]\right.$$
$$\left. - K_{mn}V(m) - K_{nm}V(n)\right\}. \tag{29}$$

The curvature parameters K_{ij}, the geometric coefficients α_{ij}, b_i^j, and g^{ij}, and the Jacobian J which appear in the above equations are functions of the coordinates only. When either analytic or numerical transformations are employed to generate the grid distribution, their values can be readily evaluated in the transformed plane.

It should be recalled that $V(i) = (U, V, W)$ are the velocity components in the direction of the orthogonal curvilinear coordinates (x^1, x^2, x^3, t). Equations (26), together with the equation of continuity (1), which transforms to

$$\frac{1}{J}\sum_{m=1}^{3}\sum_{n=1}^{3}\frac{\partial}{\partial \xi^m}[b_n^m V(n)] = 0 \tag{30}$$

are the Reynolds-averaged Navier–Stokes equations for unsteady, three-dimensional, turbulent flows.

Numerical Solution Procedures

(a) *Finite-Analytic Discretization for the Transport Equations*

In order to correctly handle the elliptic nature of the flow, the finite-analytic method of Chen and Chen [29–31] is revised and extended to solve the five trans-

port equations for mean velocities (U, V, W) and turbulence quantities (k, ε) for three-dimensional flows. The most general version of this method would involve an analytic solution of the linearized transport equations in a three-dimensional element and would result in a 28-point discretization formula. While such a scheme may be required for the solution of highly three-dimensional flows in which there is no preferred or predominant flow direction, for applications to many aerodynamic and hydrodynamic problems it suffices to use a simplified method to reduce computer time and storage. Here, we adopt a hybrid method which combines a two-dimensional local analytic solution in the $\eta\zeta$-plane with a one-dimensional local analytic solution in the ξ-direction which is aligned roughly with the primary flow direction. Details of this numerical scheme are described in the following.

In the finite-analytic approach, Eqs. (26) are locally linearized in each rectangular numerical element, $\Delta\xi = \Delta\eta = \Delta\zeta = 1$, by evaluating the coefficients of the convective terms at the interior node P of each local element (Fig. 2), i.e.,

$$g_P^{11}\phi_{\xi\xi} + g_P^{22}\phi_{\eta\eta} + g_P^{33}\phi_{\zeta\zeta} = 2(a_\phi^1)_P\phi_\xi + 2(a_\phi^2)_P\phi_\eta + 2(a_\phi^3)_P\phi_\zeta + (R_\phi)_P\phi_\tau + (S_\phi)_P. \quad (31)$$

Introduction of the coordinate-stretching functions

$$\xi^* = \xi/\sqrt{g_P^{11}}, \qquad \eta^* = \eta/\sqrt{g_P^{22}}, \qquad \zeta^* = \zeta/\sqrt{g_P^{33}} \quad (32)$$

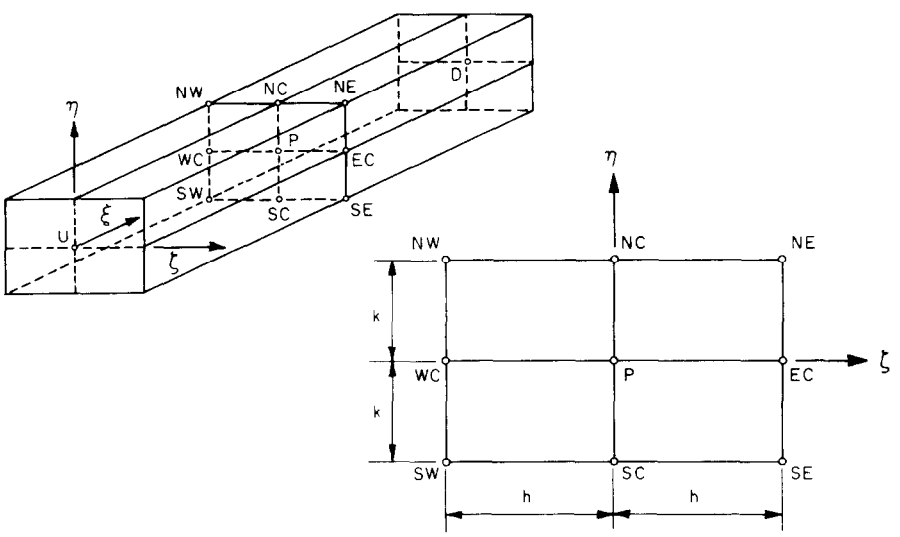

FIG. 2. Local numerical element.

in Eq. (31) reduces it to the standard three-dimensional convective-transport equation described in Chen and Chen [29, 31], i.e.,

$$\phi_{\xi^*\xi^*} + \phi_{\eta^*\eta^*} + \phi_{\zeta^*\zeta^*} = 2C\phi_{\xi^*} + 2B\phi_{\eta^*} + 2A\phi_{\zeta^*} + R\phi_\tau + (S_\phi)_P, \tag{33}$$

where

$$A = (a_\phi^3)_P/\sqrt{g_P^{33}}, \qquad B = (a_\phi^2)_P/\sqrt{g_P^{22}}, \qquad C = (a_\phi^1)_P/\sqrt{g_P^{11}}, \qquad R = (R_\phi)_P$$

for a numerical element with dimensions

$$\Delta\xi^* = l = (\sqrt{g_P^{11}})^{-1}, \qquad \Delta\eta^* = k = (\sqrt{g_P^{22}})^{-1}, \qquad \Delta\zeta^* = h = (\sqrt{g_P^{33}})^{-1}. \tag{34}$$

For the type of applications considered here, it is convenient to decompose Eq. (33) into a one-dimensional and a two-dimensional partial differential equation,

$$2C\phi_{\xi^*} - \phi_{\xi^*\xi^*} + R_\phi\phi_t + S_\phi = G(\xi^*, \eta^*, \zeta^*, \tau) \tag{35}$$

$$\phi_{\eta^*\eta^*} + \phi_{\zeta^*\zeta^*} - 2B\phi_{\eta^*} - 2A\phi_{\zeta^*} = G(\xi^*, \eta^*, \zeta^*, \tau), \tag{36}$$

where, as noted above, ξ is the predominant flow direction. If we require the source functions G and S_ϕ to be constant in each local element and the time derivatives to be approximated by a backward-difference formula, Eqs. (35) and (36) reduce to the standard one- and two-dimensional convective-transport equations described in Chen and Chen [29], respectively. The analytic solution of the one-dimensional equation (35) can be readily obtained as:

$$\phi = a(e^{2C\xi^*} - 1) + b\xi^* + c. \tag{37}$$

By substituting the exponential-linear solution (37) into Eq. (35), the source function $G(0, 0, 0, 0) = g$ becomes

$$\begin{aligned} g &= (2C\phi_{\xi^*} - \phi_{\xi^*\xi^*} + R_\phi\phi_t + S_\phi)_P \\ &= (C_U + C_D)\,\phi_P - C_U\phi_U - C_D\phi_D + \frac{R}{\Delta\tau}(\phi_P - \phi_P^{n-1}) + (S_\phi)_P \end{aligned} \tag{38}$$

with

$$C_U = \frac{Ce^{Cl}}{l\sinh Cl}, \quad C_D = \frac{Ce^{-Cl}}{l\sinh Cl},$$

where the subscripts U and D denote the upstream and downstream nodal values (Fig. 2), respectively, superscript $(n-1)$ denotes the value at the previous time step, and $\Delta\tau$ is the time step.

By specifying a combination of exponential and linear boundary functions, which are derived from the natural solutions of the governing equations, on all four boundaries, $\eta^* = \pm k$ and $\zeta^* = \pm h$, of the transverse section of each local element

(ξ-plane), the two-dimensional equation (36) can be solved analytically by the method of separation of variables or any other analytic technique. Details of the solution procedure are described in Chen and Chen [29, 30]. When the local analytic solution thus derived is evaluated at the central node P of the element, the following nine-point finite-analytic algebraic equation is obtained,

$$\phi_P = C_{NE}\phi_{NE} + C_{NW}\phi_{NW} + C_{SE}\phi_{SE} + C_{SW}\phi_{SW} + C_{EC}\phi_{EC} + C_{WC}\phi_{WC} + C_{NC}\phi_{NC} + C_{SC}\phi_{SC} - C_P g, \tag{39}$$

where the finite-analytic coefficients C_{NE}, C_{NC}, etc. are given in Chen and Patel [23].

By substituting the nonhomogeneous term g from Eq. (38) into Eq. (39), a 12-point finite-analytic formula for unsteady, three-dimensional, elliptic equations can be obtained in the form

$$\phi_P = \frac{1}{1 + C_P[C_U + C_D + R/\Delta\tau]} \left\{ \sum_1^8 C_{nb}\phi_{nb} + C_P\left(C_U\phi_U + C_D\phi_D + \frac{R}{\Delta\tau}\phi_P^{n-1} \right) - C_P(S_\phi)_P \right\}, \tag{40}$$

where the subscript nb denotes neighboring nodes (NE: northeast, NW: northwest, etc.). It is seen that ϕ_P depends upon all the eight neighboring nodal values in the transverse plane as well as the values at the upstream and downstream nodes ϕ_U and ϕ_D, and the values at the previous time step ϕ_P^{n-1}. When the cell Reynolds number $2C$ becomes large, $C_U \to 2C/l$ and $C_D \to 0$, and Eq. (40) reduces to the partially-parabolic formulation of Chen and Patel [23] which used $C_U = 2C/l$ and $C_D = 0$.

Since Eqs. (40) are implicit, both in space and time, at the current station of calculation, their assembly for all elements results in a set of simultaneous algebraic equations. These equations are solved by Jacobi line iterations with the tridiagonal-matrix algorithm. For steady-state calculations where a time-accurate solution is not needed, it is possible to use a large time step and relax the convergence criterion for intermediate solutions with only a few internal iterations at each time step. Furthermore, the finite-analytic coefficients appearing in Eqs. (40) are not updated during these internal iterations for economy of computation time.

(b) *Solution of the Continuity Equation: Velocity-Pressure Coupling*

If the pressure is known, Eqs. (40) can be employed to solve Eqs. (26) for U, V, W, k, and ε. However, the pressure is not known a priori and must be determined by requiring the velocity field to satisfy the equation of continuity (30). Since a direct method for the simultaneous solution of all six equations is not feasible with present computer capacity, it is necessary to convert the equation of continuity

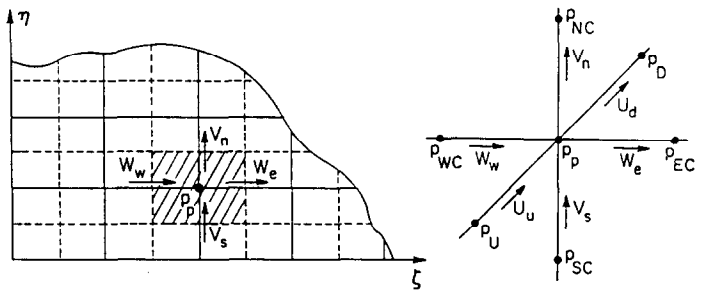

FIG. 3. Locations of the nodes for U, V, W, and p in the staggered grid.

into an algorithm for the calculation of the pressure field. The SIMPLER algorithm of Patankar [18] has been modified and extended for this purpose. A staggered-grid system is adopted. Figure 3 shows the locations of the nodes for U, V, W, and p in this grid. The turbulence quantities k and ε are evaluated at the pressure nodes. The dashed lines represent the control volume faces, and the pressure is calculated at the center of the control volume. For convenience, U_d, V_n, W_e, and p_P in Fig. 3 are assigned the same index, i.e., they are denoted by $U_{\xi\eta\zeta}$, $V_{\xi\eta\zeta}$, $W_{\xi\eta\zeta}$, and $p_{\xi\eta\zeta}$, respectively. Recall that the velocity components U, V, and W are in the preselected orthogonal curvilinear coordinate directions. In other words, they are, in general, neither perpendicular to the control surfaces nor in the direction of the coordinate lines. However, with a proper choice of the orthogonal curvilinear coordinates in the physical plane, these components will not become parallel to the control surfaces.

The 12-point finite-analytic formula (Eq. (40)) for the momentum equations is used to evaluate the velocity components (U_d, V_n, W_e) at the nodes d, n, and e in Fig. 3. These contain the pressure-gradient terms inside the source functions. An equation for this unknown pressure field is obtained as follows.

The actual velocity field (U, V, W) is decomposed into a pseudovelocity field ($\tilde{U}$, $\tilde{V}$, $\tilde{W}$) plus the pressure-gradient terms contained in the source functions, i.e.,

$$
\begin{aligned}
U_d &= \tilde{U}_d - \frac{C_d}{1 + C_d(C_U + C_D + R_U/\Delta\tau)_d}\left\{\frac{R_U}{J}(b_1^1 p_\xi + b_1^2 p_\eta + b_1^3 p_\zeta)\right\}_d \\
V_n &= \tilde{V}_n - \frac{C_n}{1 + C_n(C_U + C_D + R_V/\Delta\tau)_n}\left\{\frac{R_V}{J}(b_2^1 p_\xi + b_2^2 p_\eta + b_2^3 p_\zeta)\right\}_n \qquad (41) \\
W_e &= \tilde{W}_e - \frac{C_e}{1 + C_e(C_U + C_D + R_W/\Delta\tau)_e}\left\{\frac{R_W}{J}(b_3^1 p_\xi + b_3^2 p_\eta + b_3^3 p_\zeta)\right\}_e,
\end{aligned}
$$

so that the pseudovelocities contain no pressure terms. An equation for pressure can then be derived by requiring the velocity field to satisfy the discretized equation of continuity (30). However, with nonorthogonal coordinates, the resulting pressure equation contains many pressure nodes (see Muraoka [32], for example). It is

therefore desirable to simplify the algorithm by introducing the modified pseudo-velocities $(\hat{U}, \hat{V}, \hat{W})$,

$$\begin{aligned} U_d &= \hat{U}_d - d_d(p_D - p_P) \\ V_n &= \hat{V}_n - d_n(p_{NC} - p_p) \\ W_e &= \hat{W}_e - d_e(p_{EC} - p_P), \end{aligned} \tag{42}$$

where

$$d_d = \frac{(R_U b_1^1)_d C_d}{J_d[1 + C_d(C_U + C_D + R_U/\Delta\tau)_d]}$$

$$d_n = \frac{(R_V b_2^2)_n C_n}{J_n[1 + C_n(C_U + C_D + R_V/\Delta\tau)_n]}$$

$$d_e = \frac{(R_W b_3^3)_e C_e}{J_e[1 + C_e(C_U + C_D + R_W/\Delta\tau)_e]}$$

$(\hat{U}, \hat{V}, \hat{W})$ still contain part of the pressure-gradient terms when the coordinate system is nonorthogonal (i.e., $b_i^j \neq 0$ for $i \neq j$, see Eq. 41). These terms can be evaluated from the pressure field known at the previous time step or iteration without losing any accuracy or generality. If we require the velocity field to satisfy the equation of continuity, a simpler pressure equation can be derived in terms of the modified pseudovelocities $(\hat{U}, \hat{V}, \hat{W})$. In general, the continuity equation contains 18 velocity components for each control volume. However, due to the staggered grid system employed here, only six of these, namely, U_d, U_u, V_n, V_s, W_e, and W_w, can be obtained directly from Eqs. (41). A simple linear interpolation is used here to evaluate the remaining twelve from the velocity field known at the previous time step or iteration. The resulting equation for pressure is then

$$a_P p_P = a_d p_D + a_u p_U + a_n p_{NC} + a_s p_{SC} + a_e p_{EC} + a_w p_{WC} - \hat{D}, \tag{43}$$

where

$$a_d = (b_1^1)_d d_d, \qquad a_u = (b_1^1)_u d_u, \qquad a_n = (b_2^2)_n d_n$$
$$a_s = (b_2^2)_s d_s, \qquad a_e = (b_3^3)_e d_e, \qquad a_w = (b_3^3)_w d_w$$

$$a_P = a_d + a_u + a_e + a_w + a_n + a_s$$

$$D_1 = (b_2^1 V + b_3^1 W)_d - (b_2^1 V + b_3^1 W)_u + (b_1^2 U + b_3^2 W)_n - (b_1^2 U + b_3^2 W)_s + (b_1^3 U + b_2^3 V)_e - (b_1^3 U + b_2^3 V)_w$$

$$\hat{D} = (b_1^1 \hat{U})_d - (b_1^1 \hat{U})_u + (b_2^2 \hat{V})_n - (b_2^2 \hat{V})_s + (b_3^3 \hat{W})_e - (b_3^3 \hat{W})_w + D_1$$

The modified pseudovelocitities $(\hat{U}, \hat{V}, \hat{W})$ contain the neighboring nodal values of velocity, source functions, and part of the pressure-gradient terms. All of them

can be evaluated from the information known at the previous time step or iteration. Therefore, apart from the interpolations noted above, Eq. (43) is an exact algebraic representation of the equation of continuity. Thus, the pressure field can be obtained directly from an estimated velocity field.

Although the guessed pressure field can be updated directly by Eq. (43), in practice the new pressure field may produce a velocity field which does not satisfy the equation of continuity. An iterative procedure is therefore required to correct the velocity field for more rapid convergence. Here, a velocity-correction formula, similar to that used in the older SIMPLE algorithm, is derived in terms of the pressure-corrections,

$$a_P p'_P = a_d p'_D + a_u p'_U + a_n p'_{NC} + a_s p'_{SC} + a_e p'_{EC} + a_w p'_{WC} - D^* \tag{44}$$

with $D^* = (b_1^1 U^*)_d - (b_1^1 U^*)_u + (b_2^2 V^*)_n - (b_2^2 V^*)_s + (b_3^3 W^*)_e - (b_3^3 W^*)_w + D_1$, where (U^*, V^*, W^*) is the imperfect velocity field obtained from the imperfect pressure field p^*, and p' ($\equiv p - p^*$) is the pressure correction. The improved velocity field based on this correction is then given by

$$\begin{aligned} U_d &= U_d^* - d_d(p'_D - p'_P) \\ V_n &= V_n^* - d_n(p'_{NC} - p'_P) \\ W_e &= W_e^* - d_e(p'_{EC} - p'_P). \end{aligned} \tag{45}$$

Note that the pressure-correction equation (44) is similar to the pressure equation (43). Although, unlike the pressure equation, the pressure-correction equation is not exact, the approximations made influence only the rate of convergence but not the final converged solution.

The system of algebraic equations formed by the assembly of Eqs. (43) and (44) is solved by Jacobi line iterations with the tridiagonal-matrix algorithm. The finite-analytic coefficients a_P, a_d, etc., are updated in each upstream to downstream global sweep, but remain the same during the internal iterations.

(c) *Summary of Solution Procedure*

For transient problems, where the initial and boundary conditions are properly specified, the overall numerical solution procedure is as follows:

1. Construct the coordinate system for the given body shape and solution domain, and calculate the geometric coefficients b_i^j, g^{ij}, J, etc. from Eqs. (22) to (25).

2. Specify the initial conditions for the velocity and turbulence fields. Set $p = 0$ everywhere initially.

3. Specify the velocity and turbulence profiles at the first station $\xi = 1$ (these may be time dependent).

4. Calculate the finite-analytic coefficients for momentum, pressure, and pressure-correction equations at the downstream station from Eqs. (39) and (43),

respectively. Store only the finite-analytic coefficients a_d, a_n, and a_e for the pressure equation.

5. Solve the momentum equations based on the updated pressure field to obtain the starred velocity field (U^*, V^*, W^*).

6. Calculate the mass source D^*, and solve the pressure-correction equation (44).

7. Correct the velocity field using the velocity-correction formulae (45), but do not correct the pressure field.

8. Update wall-function boundary conditions using the newly-obtained velocity field and repeat steps 5 to 7 for several internal iterations.

9. Calculate the pseudovelocities ($\hat{U}$, $\hat{V}$, $\hat{W}$) in terms of the velocity field from Eq. (42). Store only $\hat{D}$ for later use.

10. Solve Eqs. (40) for turbulence quantities ($\phi = k, \varepsilon$).

11. March to the next downstream station and repeat steps 4 to 10.

12. After reaching the last downstream station, solve the pressure equation (43). Several iterations from downstream to upstream are employed to update the three-dimensional elliptic pressure field. Depending upon the time step employed, some under-relaxation of pressure is required for convergence.

13. Repeat steps 4 to 12 for several sweeps until both the pressure and

14. Return to step 3 for the next time step.

Example Application

Many basic components of the present numerical method have been subjected to critical tests and validations. Extensive comparisons with known analytical results, other numerical solutions, and well-established data sets have been made for laminar and turbulent flows on simple two-dimensional and axisymmetric flows [33–37] to gauge the overall accuracy of the method. However, the full capability of the method remains to be demonstrated for applications involving practical three-dimensional geometries. In the following, we present solutions for the flow over the stern and in the wake of a typical ship hull, namely the SSPA 720 Cargo Liner. Measurements of the boundary layer on a double model of this hull form were made by Larsson [38] in a wind tunnel. The data were supplemented by corresponding turbulence measurements by Löfdahl [39] and Löfdahl and Larsson [40].

(a) *Coordinates*

As noted earlier, the present method can be used with either analytic or numerical coordinate transformations. For the application to a ship hull considered here,

we use a numerically-generated body-fitted coordinates system, since it offers the advantages of generality and flexibility and, most importantly, allows a more direct control of grid distributions in regions requiring higher resolution. The grid-generation technique employed here is based on the solution of a system of Poisson equations of the form of

$$\nabla^2 \xi^i = f^i, \tag{46}$$

where $\xi^1 = \xi$, $\xi^2 = \eta$, $\xi^3 = \zeta$, and ∇^2 is the Laplacian in orthogonal coordinates x^i as defined in Eq. (3). The nonhomogeneous source functions f^i may be assigned appropriate values to yield desired concentration of coordinate surfaces. In practical applications, the inverse transformation of Eq. (46) is used to obtain the coordinate transformation relations $x^i = x^i(\xi, \eta, \zeta, \tau)$, i.e.,

$$\nabla^2 x^i = \frac{1}{h_1 h_2 h_3} \frac{\partial}{\partial x^i} \left(\frac{h_1 h_2 h_3}{h_i^2} \right), \tag{47}$$

where ∇^2 is the Laplacian operator in the transformed plane (ξ, η, ζ, τ) and is defined in Eq. (20). Equations (47) were solved by an exponential-linear scheme described in Chen and Patel [23]. Some views of the grid generated in this manner are shown in Fig. 4.

As discussed in Chen and Patel [23], the cylindrical polar coordinates $(x^1, x^2, x^3) = (x, r, \theta)$ are perhaps the most convenient for the description of the flow field around ship forms. With this choice, the governing equations and the associated geometric coefficients are greatly simplified, since the only nonzero K_{ij} and α_{ij} are $K_{32} = 1/r$, and $\alpha_{22} = \alpha_{33} = -1/r^2$. The equations in cylindrical polar coordinates are given in Chen and Patel [23] and Patel, Chen, and Ju [41].

(b) *Boundary Conditions*

For the calculation of ship stern and wake flows, it is assumed that the ship is symmetric about a vertical centerplane and the waterplane is regarded as a plane of symmetry, and the solution is sought in a domain downstream of some initial section around midship where the boundary layer is thin. Referring to the physical solution domain shown in Fig. 5, the appropriate boundary conditions are then as follows:

(1) Inlet plane A ($\xi = 1$): U, V, W, k, ε specified.

(2) Exit plane B: $p_\xi = U_{\xi\xi} = V_{\xi\xi} = W_{\xi\xi} = k_{\xi\xi} = \varepsilon_{\xi\xi} = 0$.

(3) Body surface S ($\eta = 1$): two-point wall-functions.

(4) Outer boundary $\sum$: $U = 1$, $k_\eta = \varepsilon_\eta = p = 0$.

(5) Symmetry planes C, W: $U_\zeta = V_\zeta = k_\zeta = \varepsilon_\zeta = 0$; $W = 0$.

(6) Initial conditions: U, V, W, k, ε specified; $p = 0$.

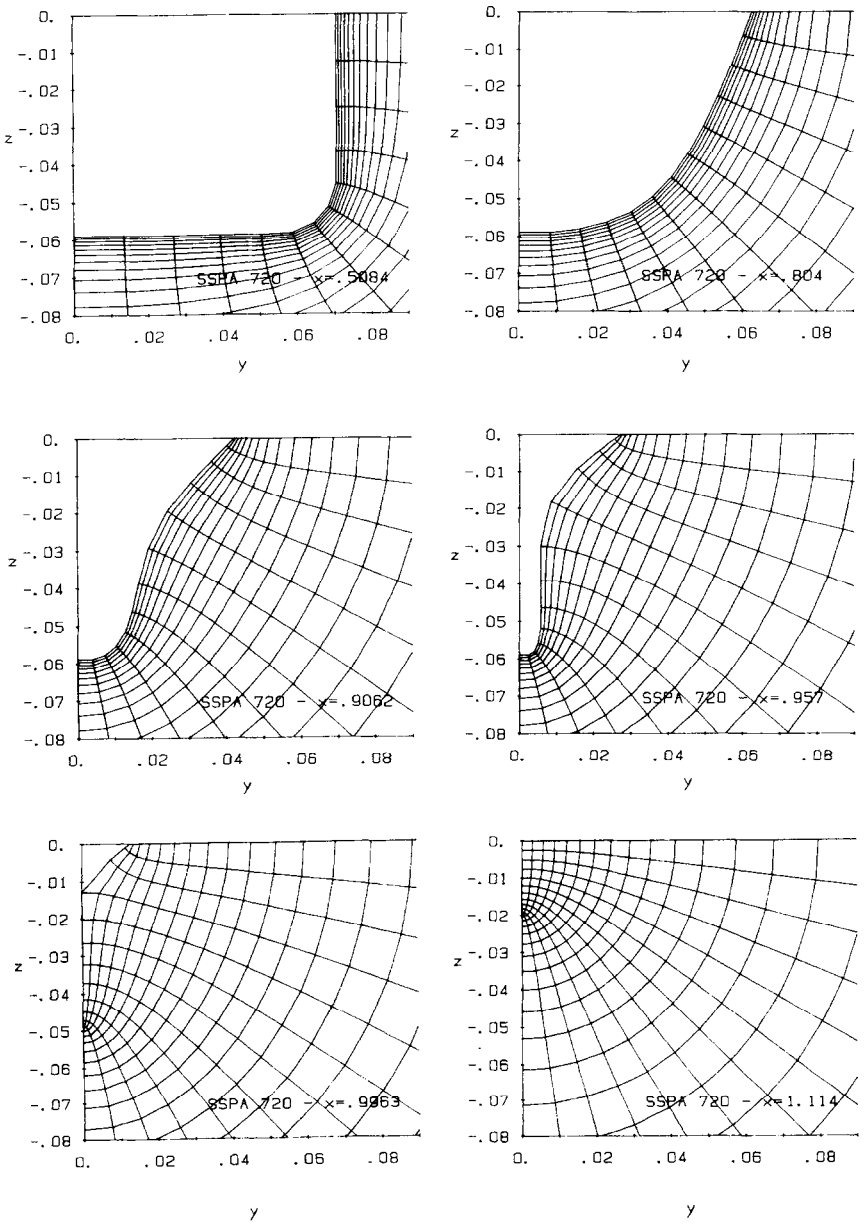

FIG. 4. Typical views of the numerical grid (six transverse sections).

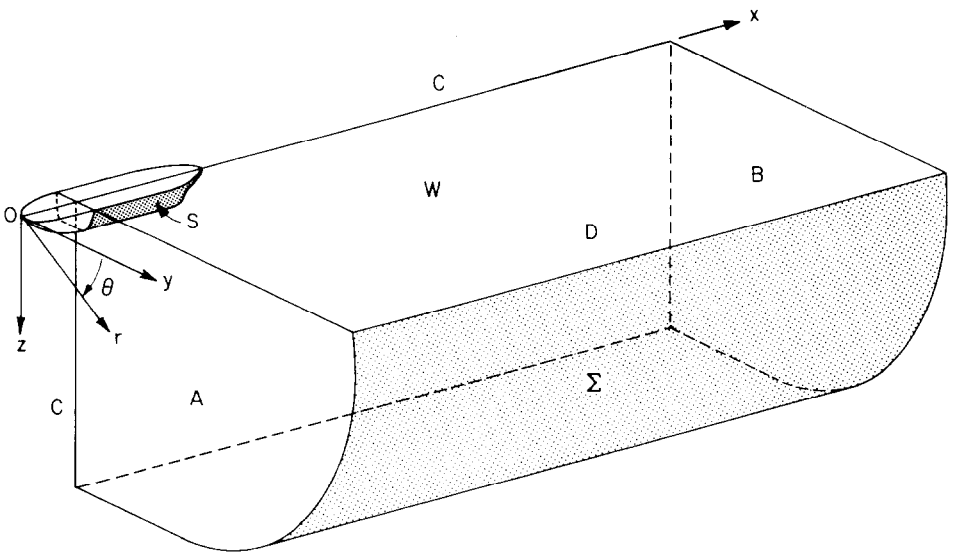

FIG. 5. Solution domain for ship stern and wake flow.

The exit boundary conditions are satisfied by linear extrapolation of known (previous iterations) values to the exit plane. The solutions are insensitive to the extrapolation if the exit plane is sufficiently far downstream. The wall-functions employed here are determined by requiring the first two points ($\eta = 2$ and 3) in the near-wall region to satisfy the generalized law of the wall given by Patel [42]. This two-point wall-function approach is described in detail in [36, 41].

Calculations for SSPA 720 Cargo Liner were performed at a Reynolds number of 5×10^6, based on model length. Several different numerical grids and solution domains were used to examine the sensitivity of the solutions to grid refinement and domain size. In addition, the convergence histories of the solutions were also examined to evaluate the overall performance of the method. We shall briefly describe the numerical as well as physical aspects of the method in the following sections.

(c) *Convergence*

Two important measures of the performance of an iterative numerical method such as the present one are the number of iterations required to obtain a converged solution and the influence of the grid. Here, we shall examine first the convergence history of several representative quantities for a typical calculation with a $(50 \times 30 \times 15)$ grid in the (x, r, θ) directions. In this particular application, as well as in all others, the calculations were performed for 160 time steps (or sweeps) to assure full convergence of the solutions although much fewer sweeps are actually required to obtain an acceptable solution.

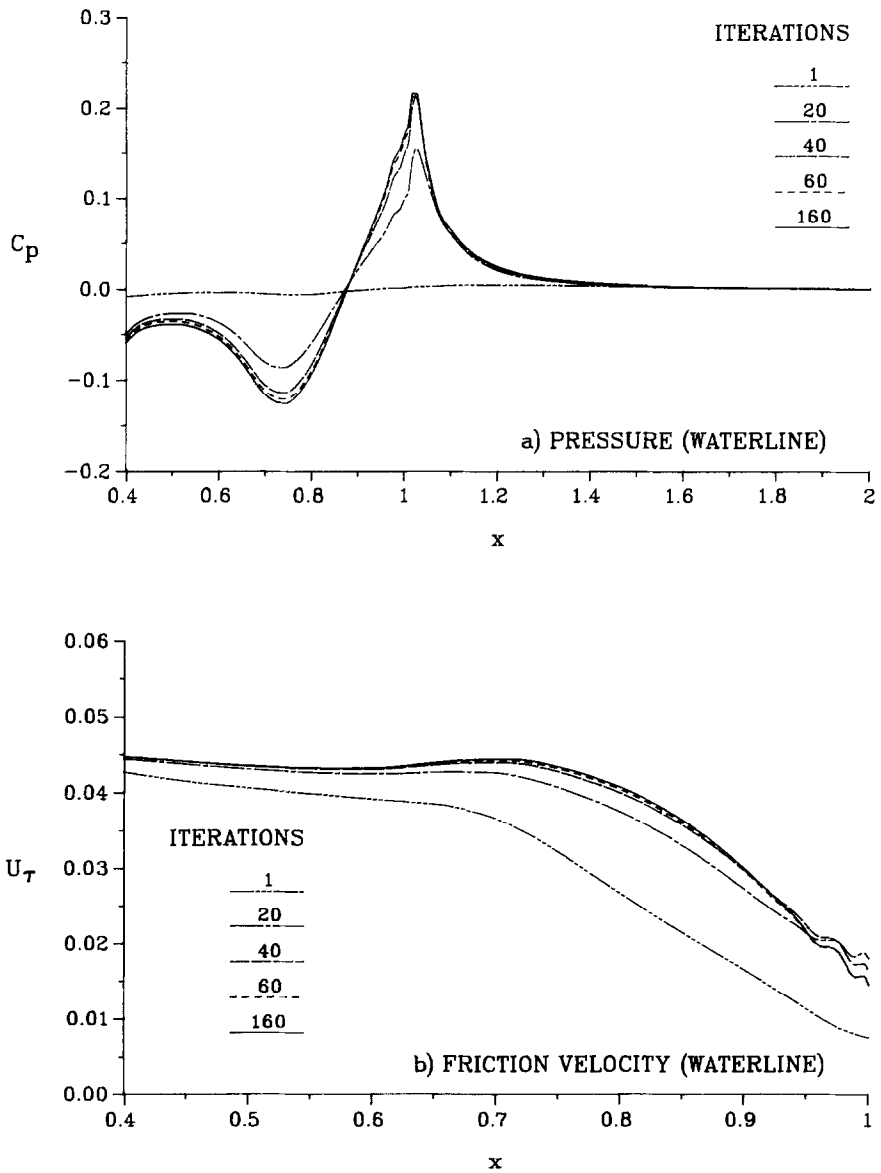

FIG. 6. Convergence history.

Figure 6 shows the convergence of the distributions of pressure, C_p ($=2p$), and friction velocity U_τ, along the waterline coordinate and its extension into the wake. It is seen that these quantities converge monotonically in less than 60 time steps or global sweeps. Recall that the solutions were started with a constant ambient pressure ($p=0$) throughout the solution domain. The calculated pressure and

velocity fields clearly capture all the important features of the final converged solutions in less than 20 sweeps. This is particularly encouraging because it eliminates the need for generating an initial pressure field from a potential-flow calculation.

Other tests of convergence of the solutions made on the velocity components, turbulence parameters, and the mass-source terms appearing in the pressure and pressure-correction equations also showed monotonic convergence similar to that depicted for the flow parameters shown in the above figures.

(d) *Grid Dependence*

Calculations were performed with four different (x, r, θ) grids in the solution domain: $\{0.3 < x < 4.5,\ r_s < r < 1.0,\ 0 < \theta < \pi/2\}$ to examine the sensitivity of the numerical solutions to grid refinement. Some information on these calculations is given in Table I. In the stern and near wake regions, the finest grid, $(74 \times 30 \times 21)$, has nearly twice as many nodes in each direction compared with the coarsest one, $(41 \times 15 \times 12)$. The coarsest grid calculation converged in only 15 iterations and required only about 40 cpu seconds on the CRAY YMP/48. On the other hand, the finest grid calculation required 110 iterations and about 1830 cpu seconds. This is due to the significant increase of the number of grid nodes as well as the number of global sweeps (110) needed for convergence. We note that the computing times also vary due to the differing levels of vectorization effected by the CRAY. For the same level of vectorization, it is found that the computing time is approximately proportional to the square of the number of total nodes.

Figure 7 shows the results obtained with the four grid arrangements with regard to the flow parameters considered before. It is quite evident that the three finer grids yield nearly identical results. On the other hand, the solution with the coarsest grid shows some departure from the other three. This is presumably due to an

TABLE I

Summary of Grid Dependence Tests

Case ⇒	I	II	III	IV
Grid points				
in x-direction	41	74	50	74
in r-direction	15	15	30	30
in θ-direction	12	12	15	21
Total nodes	7,380	13,320	22,500	46,620
Time step, $\Delta\tau$	1.0	0.5	0.3	0.5
Memory, 10^6	0.32	0.51	0.84	1.63
cpu, s/iteration	2.6	5.3	6.0	16.6
Iterations for convergence	15	60	55	110
Total cpu (s)	40	320	330	1830

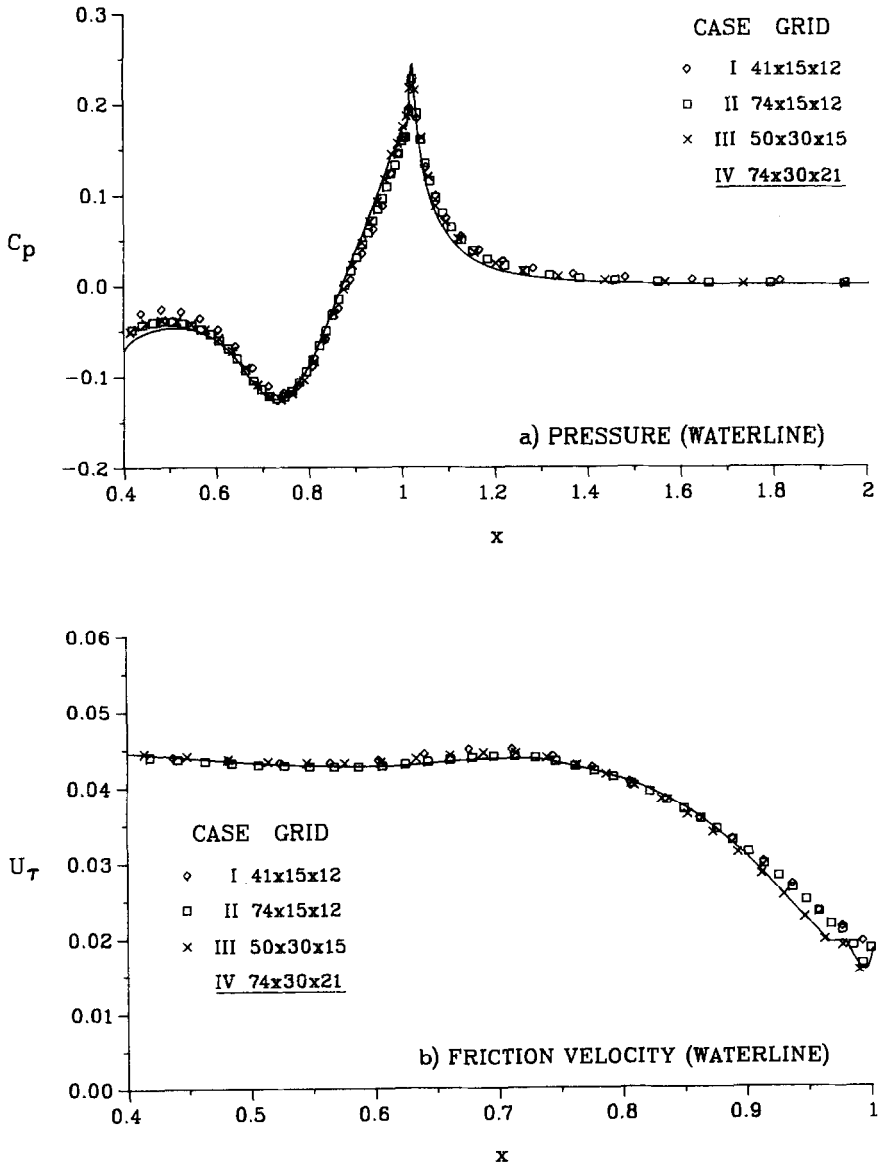

FIG. 7. Grid-dependence.

inadequate numerical resolution and less accurate specifications of boundary conditions at the hull surface and along the wake centerline. Nevertheless, it is quite encouraging to note that even the coarsest grid calculation is able to capture many of the important features of the flow which are evident from the data discussed later.

(e) *Solution Domain*

In some earlier studies of well known two-dimensional, axisymmetric, and simple three-dimensional bodies, it was found that, with the simple uniform-stream boundary conditions employed here the numerical solutions were quite sensitive to the size of the solution domain. The most critical quantity to be examined in this regard is the pressure distribution since its influence penetrates much farther into the inviscid-flow region compared to the velocity field. In order to properly capture the entire zone of viscous–inviscid interaction, the outer boundary should be placed at a distance sufficiently far away from the body such that the uniform flow and zero pressure conditions are indeed appropriate. Similarly, the downstream boundary must be located in the far wake where upstream propagation of pressure becomes negligible.

For the present applications to ship stern and wake flows, we have varied the location of the outer and downstream boundaries over a wide range to examine the influence of domain size on the solutions. Calculations were performed for four different combinations of downstream and outer boundaries, namely,

$0.3 < x < 23.1,\ r_s < r < 2.00$ with a $(57 \times 35 \times 15)$ grid,

$0.3 < x < 4.53,\ r_s < r < 0.95$ with a $(50 \times 31 \times 15)$ grid,

$0.3 < x < 1.95,\ r_s < r < 0.47$ with a $(45 \times 27 \times 15)$ grid,

$0.3 < x < 1.34,\ r_s < r < 0.22$ with a $(41 \times 22 \times 15)$ grid.

The grids for the three smaller domains were obtained by simply deleting an appropriate number of outer and downstream grid lines from the grid generated for the largest solution domain. Therefore, the four solutions correspond to essentially the same grid distributions. It is seen from Fig. 8 that the solutions with the two larger domains are essentially the same. It is also clear that the smallest domain is too small to correctly predict the pressure distribution over the hull. These calculations suggest that domain dependency can be eliminated by choosing an outer boundary which is farther than about a half ship length from the axis, and the downstream boundary at a similar distance from the stern.

(f) *Results and Comparisons with Experiments*

A detailed description of the numerical results obtained by the present method for a variety of hull forms, including the present case, is given in Patel, Chen, and Ju [4]. Here, we shall examine only a few selected results to demonstrate the capability and overall performance of the method. In this regard, we note that the most critical quantities in gauging the success of a method for external flow applications are the pressure and shear-stress distributions on the body surface. Figure 9 shows the distribution of pressure and friction velocity U_τ along the keel and waterline planes of symmetry. It is seen that the calculated wall pressures are in quite good agreement with the data corrected for wind-tunnel blockage. The friction velocities along the keel are also in excellent agreement with the available data.

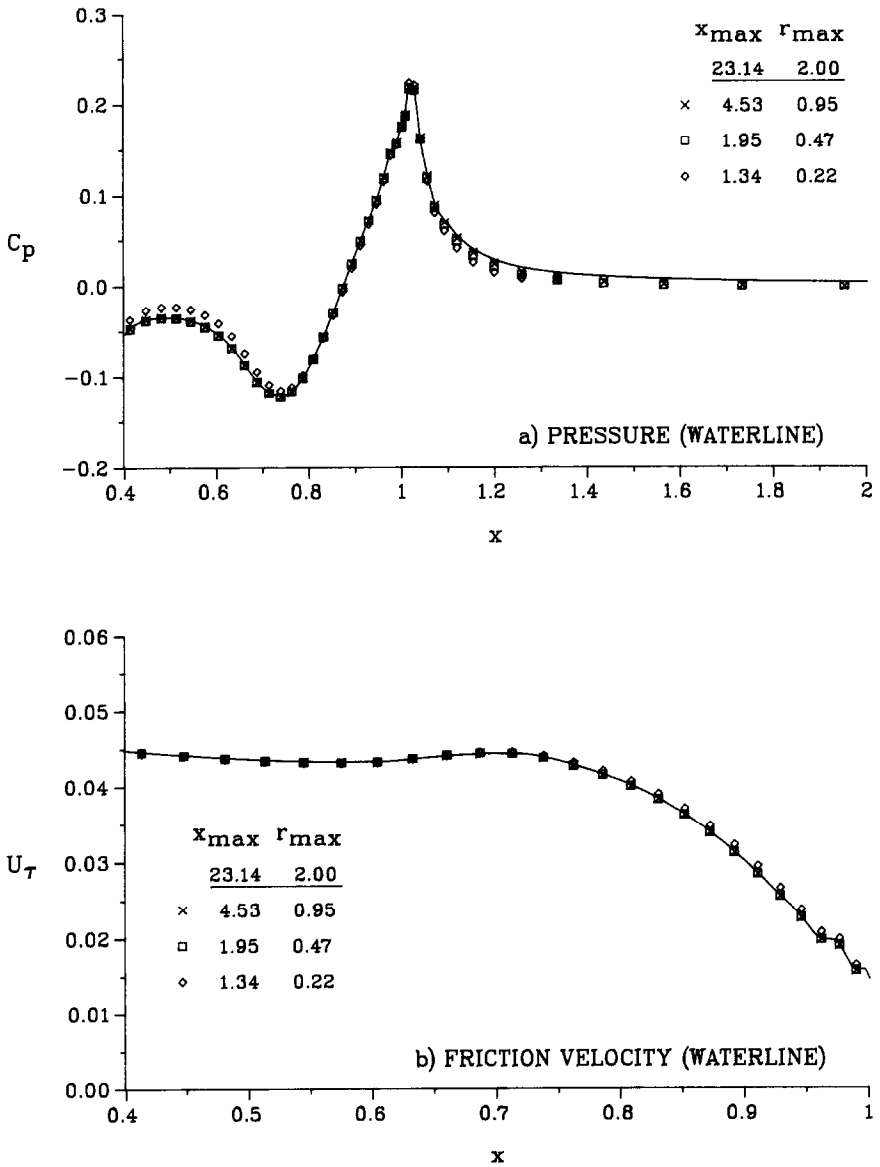

FIG. 8. Influence of solution domain size.

The same level of agreement has also been achieved for the girthwise distributions of pressure and friction velocity [41].

The development and evolution of the three-dimensional flow pattern associated with the predicted friction distribution can also be seen from the limiting streamlines on the hull surfaces. Figure 10 shows the divergence of wall streamlines

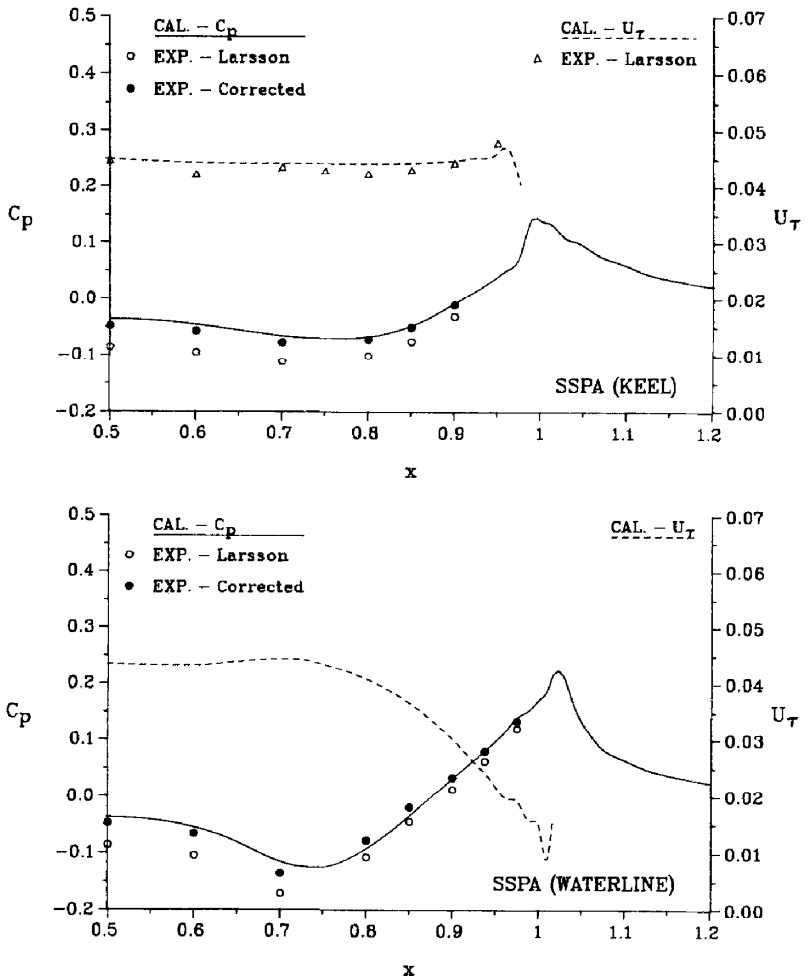

FIG. 9. Pressure and friction velocity along the keel and waterline.

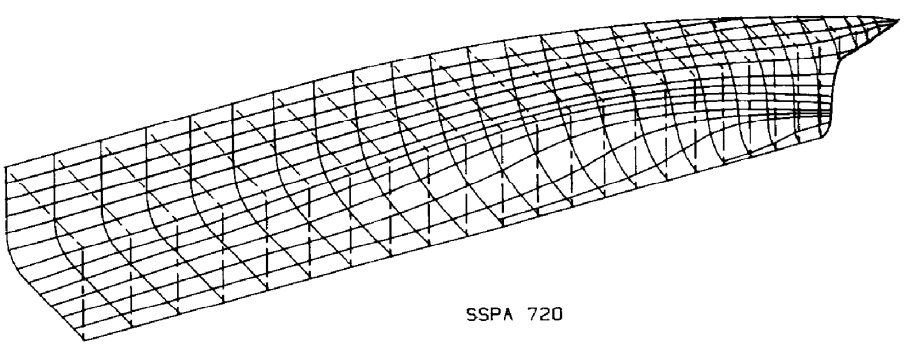

FIG. 10. Calculated wall streamlines.

out of the keel over much of the keel which results in a thinning of the boundary layer along the keel. There is also a secondary motion, although somewhat weaker, towards the midgirth low pressure region from the waterplane. This convergence of flow from both sides eventually leads to a thickening of the viscous layer around midgirth in the stern region.

The flow patterns on the waterplane and in the vertical centerplane are shown in Fig. 11. The thickening of the boundary layer over the stern in the waterplane and the thinning of the boundary layer along the keel are clearly seen from these views as is the evolution of the three-dimensional wake. Contours of the axial velocity (U) and velocity vectors projected into transverse sections (V and W components) are

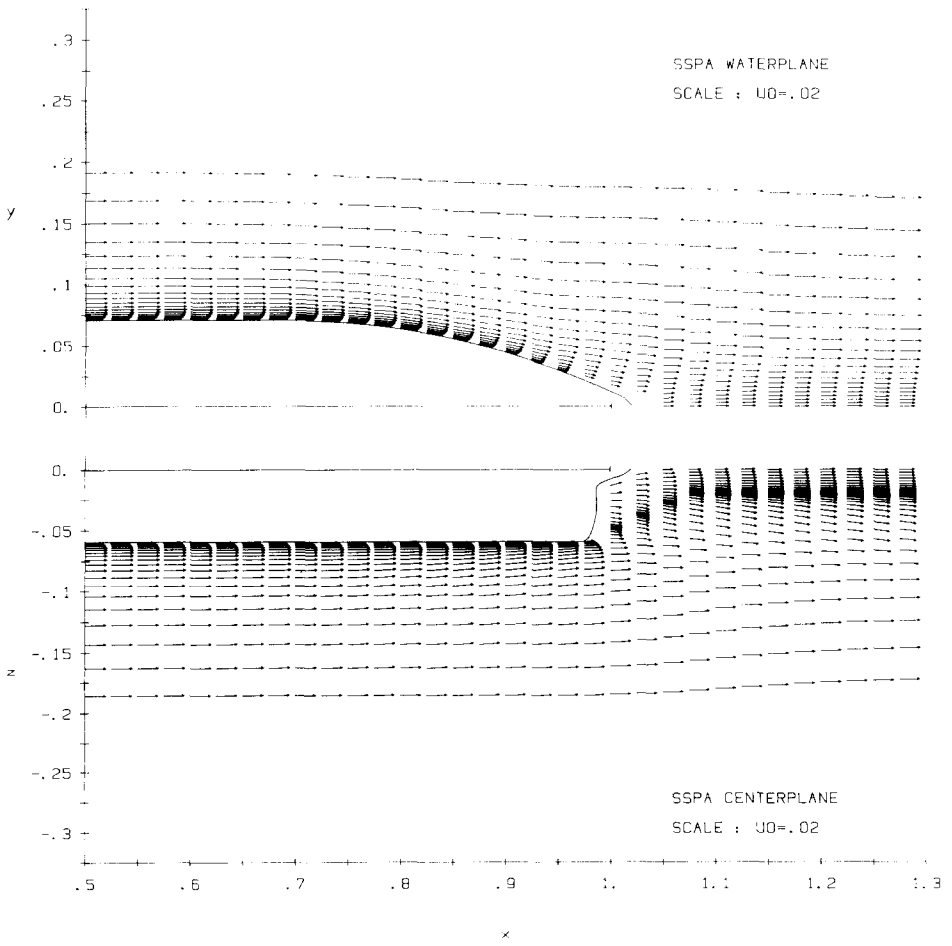

FIG. 11. Velocity vectors in the waterplane (top) and in the vertical centerplane (bottom).

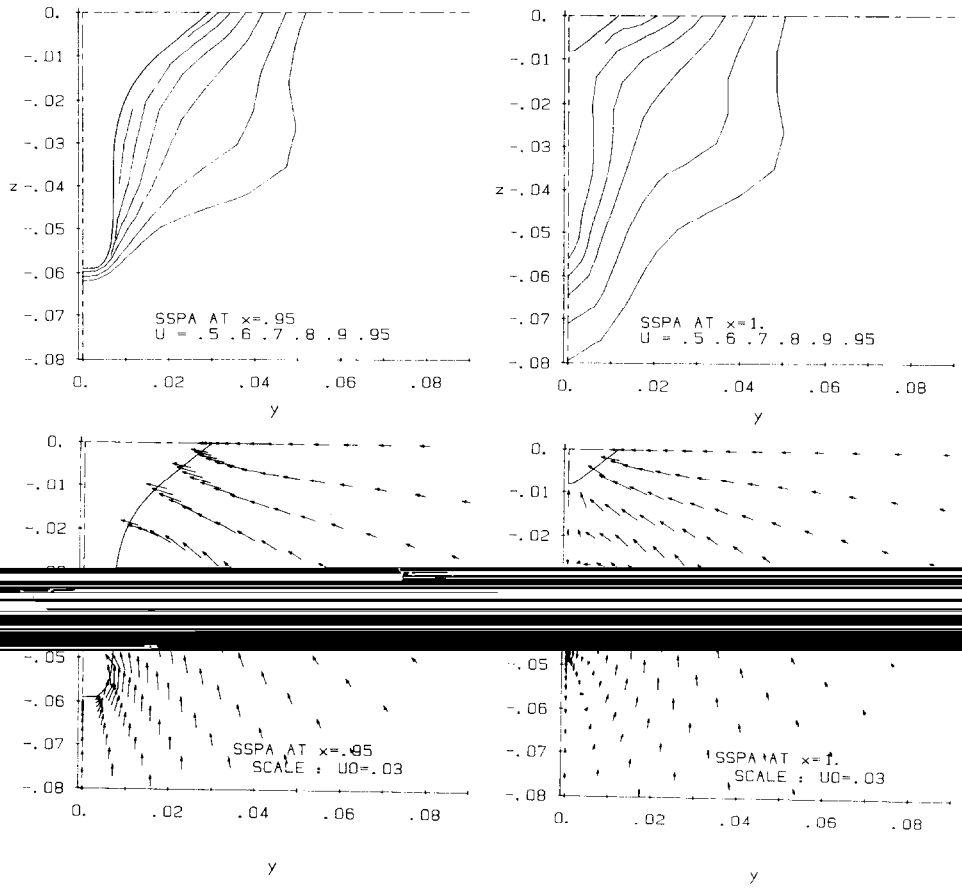

FIG. 12. Velocity field in transverse sections: (a) $x = 0.95$; (b) $x = 1.0$. Top: contours of axial velocity (U); bottom: velocity vectors in transverse sections (V, W).

shown in Fig. 12 for two representative sections in the stern region ($x = 0.95$ and 1.0). The secondary motion induced by the rapid changes in hull geometry is quite strong and converges from both the keel and waterplane towards the midgirth. This convergence is responsible for the rapid thickening of the midgirth boundary layer. At the downstream section, the secondary motion gives the impression of a longitudinal vortex, but the strength of this motion diminishes quite rapidly.

More detailed comparisons between experiments and calculations are presented in Fig. 13. The calculated results were interpolated to determine the variation, with distance N normal to the transverse section of the hull, of the resultant velocity parallel to the hull (Q), the crossflow velocity (C), and the turbulent kinetic energy (k) at $x = 0.95$, where strong three-dimensionality of the flow field is observed. We note first that the variation of the thickness of the viscous layer in the girthwise

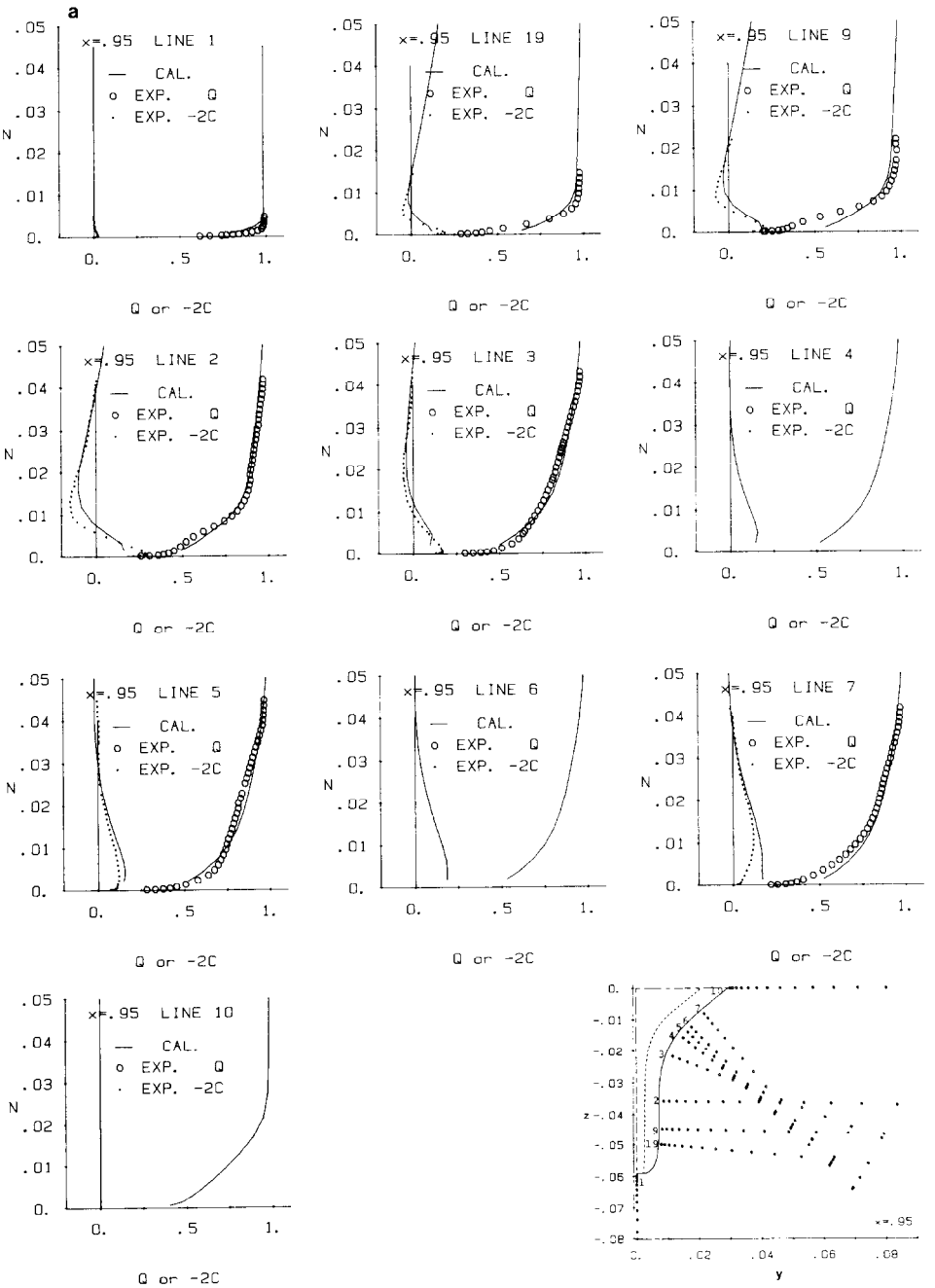

FIG. 13. Comparison between calculations and experiment at $x = 0.95$: (a) profiles of resultant velocity (Q) and crossflow velocity (C); (b) profiles of turbulent kinetic energy (k).

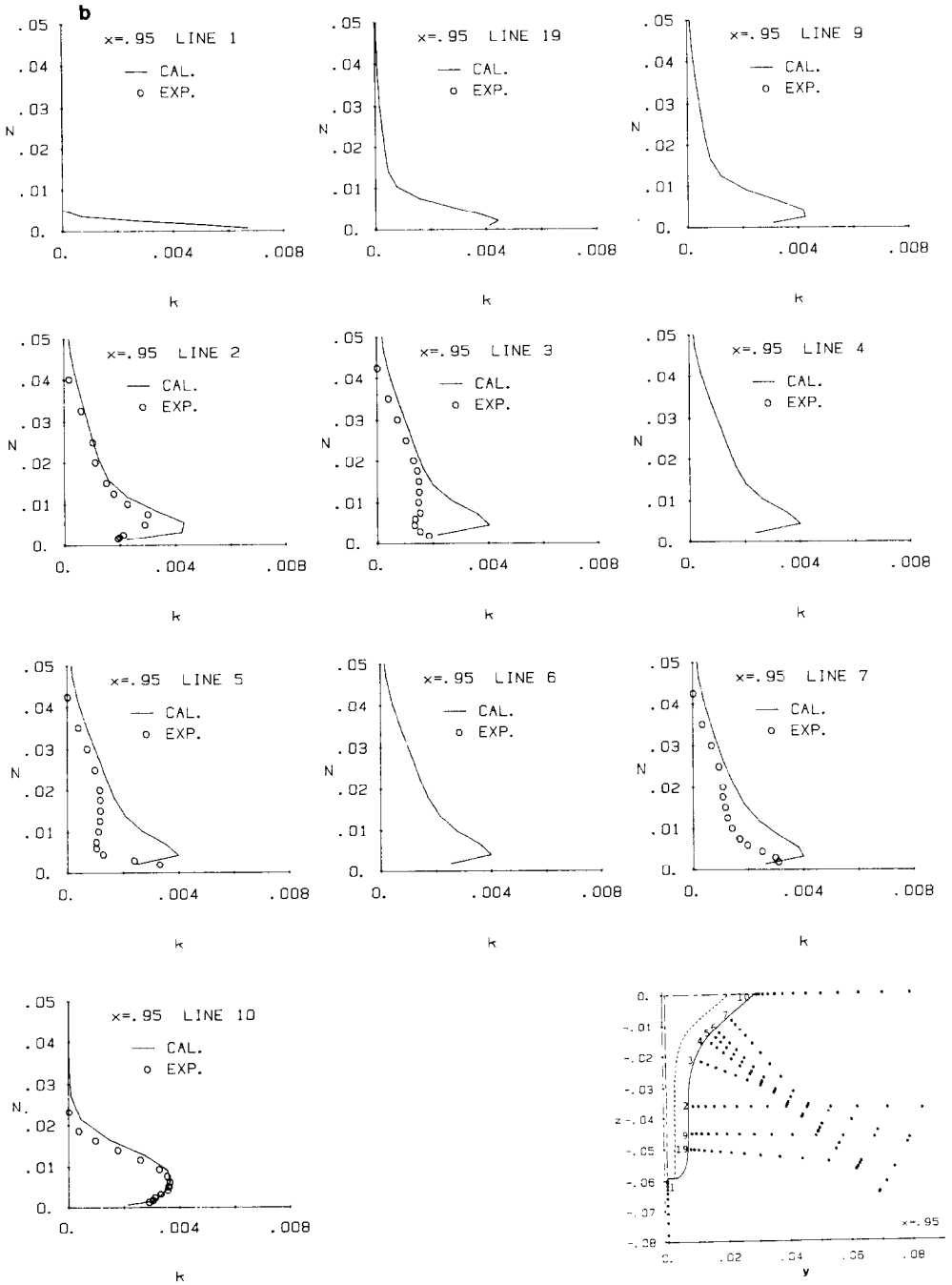

FIG. 13—*Continued*

direction is predicted with considerable accuracy. Second, the profiles of Q and C are described quite well by the calculation although there is a tendency for the calculated velocities to be somewhat higher in the near-wall region. Third, the predicted turbulent kinetic energy is considerably larger than that measured. Finally, we note a very characteristic two-layer feature developing around midgirth which suggests the existence of a thin layer of fluid close to the wall in which k diminishes rapidly, and a much larger layer farther out where there is a plateau in k and a gradual decrease to zero outside the viscous region. Although there is a hint of such a two-layer structure in the calculated profiles, it is obvious that the present turbulence model does not capture the changes that are taking place in the turbulence in the flow over the stern.

Summary and Conclusions

A fully-elliptic numerical method for the solution of the complete Reynolds-averaged Navier–Stokes equations for general three-dimensional, incompressible flows has been presented. The method uses nonorthogonal body-fitted coordinates while retaining the velocity components in an orthogonal curvilinear coordinate system. For turbulent flows, closure of the equations is effected by the well known $k-\varepsilon$ model with the generally accepted values of the constants in the model and a two-point wall-function approach. The various numerical features of the method have been described and evaluated.

Calculations have been performed for the flow over the stern and in the wake of a practical ship hull for which experimental data are available. Comparisons have been made to understand the important features of such flows and to demonstrate the full capability of the calculation method. It is quite clear from these calculations, as well as many others presented and discussed in Refs. [33–37, 41], that the present method has many attractive features. Among them are rapid and monotonic convergence to steady-state solutions starting from rather simple initial guesses, ability to perform accurate calculations over a large solution domain with a relatively modest grid, and the potential to calculate unsteady flows. It is anticipated that, with suitable modifications, the method can be utilized for the solution of other problems encountered in aero- and hydrodynamics.

Acknowledgments

The research described herein was sponsored by the Office of Naval Research, Accelerated Research Initiative Program in Ship Hydrodynamics, under Contracts N00014-83-K-0136, N00014-88-K-0001. The authors appreciate the support and encouragement of ONR Program Managers, Dr. C. M. Lee, Mr. J. Fein, and Dr. E. P. Rood during the course of this research. The Graduate College of The University of Iowa provided a large share of the computer funds utilized in the initial development of the numerical method. Its application to ship hulls was greatly facilitated by allocation of time on the CRAY XMP-24 supercomputer of the Naval Research Laboratory and on the CRAY XMP-48 machine of the National Center for Supercomputing Applications at Urbana-Champaign.

REFERENCES

1. *AIAA 8th Computational Fluid Dynamics Conference, Honolulu, HA, 1987.*
2. W. D. MCNALLY AND P. M. SOCKOL, *ASME, J. Fluids Engrg.* **107**, 6 (1985).
3. V. C. PATEL, *Proceedings*, 17th *ONR Symposium on Naval Hydrodynamics, The Hague, The Netherlands, 1988*, p. 217.
4. J. S. SHANG, *AIAA 17th Fluid Dynamics, Plasma Dynamics, and Lasers Conference, Snowmass, CO, 1984*, Paper AIAA–84–1549 (unpublished).
5. R. W. MACCORMACK, *AIAA 23rd Aerospace Sciences Meeting, Reno, NE, 1985*, Paper AIAA–85–0032 (unpublished).
6. A. JAMESON, *AIAA* 8th *Computational Fluid Dynamics Conference, Honolulu, HA, 1987*, Paper AIAA–87–1184 (unpublished).
7. J. F. NASH AND V. C. PATEL, *Three-Dimensional Turbulent Boundary Layers* (SBC Tech Books, Atlanta, 1972).
8. W. R. BRILEY AND H. MCDONALD, *J. Comput. Phys.* **24**, 372 (1977).
9. L. W. SPRADLEY, J. F. STALNAKER, AND A. W. RATLIFF, *AIAA J.* **19**, 1302 (1981).
10. J. S. SHANG, P. C. BUNING, W. L. HANKEY, AND M. C. WIRTH, *AIAA J.* **18**, 1073 (1980).
11. J. S. SHANG AND S. J. SCHERR, *AIAA* 7th *Computational Fluid Dynamics Conference, Cincinnati, OH, 1985*, Paper AIAA–85–1509 (unpublished).
12. G. V. CANDLER AND R. W. MACCORMACK, *AIAA 25th Aerospace Sciences Meeting, Reno, NE, 1987*, Paper AIAA–87–0480 (unpublished).
13. D. B. SPALDING, *Math. Comput. Simul.* **13**, 267 (1981).
14. C. M. RHIE, *AIAA 24th Aerospace Sciences Meeting, Reno, NE, 1986*, Paper AIAA–86–0207 (unpublished).
15. D. KWAK, J. L. C. CHANG, S. P. SHANKS, AND S. R. CHAKRAVARTHY, *AIAA J.* **24**, 390 (1986).
16. T. HAN, *1st National Fluid Dynamics Congress, Cincinnati, OH, 1988*, Paper AIAA–88–3766 (unpublished).
17. S. V. PATANKAR AND D. B. SPALDING, *Int. J. Heat Mass Transf.* **15**, 1787 (1972).
18. S. V. PATANKAR, *Numerical Heat Transfer and Fluid Flow* (McGraw–Hill, New York, 1980).
19. R. I. ISSA, *J. Comput. Phys.* **62**, 40 (1986).
20. A. J. CHORIN, *J. Comput. Phys.* **2**, 12 (1967).
21. C. L. MERKLE AND M. ATHAVALE, *AIAA 8th Computational Fluid Dynamics Conference, Honolulu, HA, 1987*, Paper AIAA–87–1137 (unpublished).
22. H. C. CHEN AND V. C. PATEL, *Proceedings*, 15*th ONR Symposium on Naval Hydrodynamics, Hamburg, FRG, 1984*, p. 505.
23. H. C. CHEN AND V. C. PATEL, Iowa Institute of Hydraulic Research, University of Iowa, Iowa City, IA, IIHR Report No. 285, 1985.
24. H. C. CHEN AND V. C. PATEL, *Proceedings, 4th International Conference on Numerical Ship Hydrodynamics, Washington, DC, 1985*, p. 492.
25. M. C. RICHMOND, H. C. CHEN, AND V. C. PATEL, Iowa Institute of Hydraulic Research, University of Iowa, Iowa City, IA, IIHR Report No. 300, 1986.
26. F. STERN, S. Y. YOO, AND V. C. PATEL, *AIAA J.* **26**, 1052 (1988).
27. I. DEMIRDZIC, A. D. GOSMAN, R. I. ISSA, AND M. PERIC, *Comput. Fluids* **15**, 251 (1987).
28. S. OGAWA AND T. ISHIGURO, *J. Comput. Phys.* **69**, 49 (1987).
29. C. J. CHEN AND H. C. CHEN, Iowa Institute of Hydraulic Research, University of Iowa, Iowa City, IA, IIHR Report No. 232–IV, 1982.
30. C. J. CHEN AND H. C. CHEN, *J. Comput. Phys.* **53**, 209 (1984).
31. H. C. CHEN AND C. J. CHEN, *Computation of Internal Flows: Methods and Applications, ASME Symposium, 1984*, p. 159.
32. K. MURAOKA, *Trans. West Japan Soc. Naval Arch.* **63**, 13 (1982).
33. H. C. CHEN AND V. C. PATEL, *AIAA J.* **25**, 920 (1987).
34. V. C. PATEL AND H. C. CHEN, *AIAA J.* **25**, 1078 (1987).
35. V. C. PATEL AND H. C. CHEN, *J. Ship Res.* **30**, 201 (1986).

36. H. C. CHEN AND V. C. PATEL, *AIAA J.* **26**, 641 (1988).
37. H. C. CHEN AND V. C. PATEL, *Turbulent Shear Flows* 6 (Springer-Verlag, Berlin/Heidelberg, 1988).
38. L. LARSSON, Swedish Maritime Research Center (SSPA), Goteborg, Sweden, Report No. 46, 1974.
39. L. LÖFDAHL, Doctoral thesis, Chalmers University, Goteborg, Sweden, 1982.
40. L. LÖFDAHL AND L. LARSSON, *J. Ship Res.* **28**, 186 (1984).
41. V. C. PATEL, H. C. CHEN, AND S. JU, Iowa Institute of Hydraulic Research, University of Iowa, Iowa City, IA, IIHR Report No. 323, 1988.
42. V. C. PATEL, *Aeron. Q.* **24**, 55 (1973).